

Ordered Polyelectrolyte “Multilayers”. 4. Internal Structure of Clay-Based Multilayers

K. Glinel,^{†,‡} A. Laschewsky,^{§,||} and A. M. Jonas*,[†]

Unité de Physique et de Chimie des Hauts Polymères, Université Catholique de Louvain, Place Croix du Sud, 1, B-1348 Louvain-la-Neuve, Belgium (European Union), and Département de Chimie, Université Catholique de Louvain, Place Louis Pasteur, 1, B-1348 Louvain-la-Neuve, Belgium (European Union)

Received: June 18, 2002; In Final Form: September 1, 2002

We report on the growth and structure of hybrid clay-based multilayers obtained by electrostatic self-assembly (also known as layer-by-layer assembly) of poly(diallylpyrrolidinium bromide) and a synthetic hectorite (Laponite). By combining ellipsometry, atomic force microscopy, and specular and off-specular grazing angle X-ray scattering measurements, we show that platelets pack in the vertical direction according to a distribution of distances between nearest neighbors of about 3 Å standard deviation. The accumulation of such random fluctuations in the vertical direction results in the loss of layering of the platelets farther than about 75 Å from the substrate. In this respect, most of the film should be considered as a nanocomposite with preferential orientation of the platelets, rather than as a real multilayer. The model is quantitatively supported by simulations of the specular and off-specular scattering of such multilayers.

Introduction

Layer-by-layer assembly (LBL) of polyelectrolytes (also known as electrostatic self-assembly, ESA) is a promising technique for the fabrication of thin functional films of composition controlled at the nanometer scale.^{1–3} However, as discussed repeatedly,^{1,3} the interpenetration of successively adsorbed polyelectrolyte “layers” is such that the local structure of binary (A/B)_n ESA films is closer to the one of a scrambled-egg polyelectrolyte complex^{4–6} than to the one expected for a truly layered film. Accordingly, no Bragg reflection appears in X-ray reflectograms of such LBL films, except when some special polyelectrolytes capable to form lyotropic mesophases are being used.⁷ In these exceptional cases, the intrinsic drive of the polyelectrolyte to microphase-separate or to self-organize in water is responsible for the formation of an ordered film structure extending over long distances. Nevertheless, the resulting layering does not strictly coincide with the sequence of adsorption events, with more than one stratum being deposited per dipping cycle.⁷ Still, although compositional fluctuations cannot be detected in most ESA films made from organic polyelectrolytes, such films are spatially controlled, because a given polyelectrolyte chain will be placed and remain at a vertical position strictly governed by the sequence of dipping cycles used.^{3,8}

In X-ray reflectograms, Bragg peaks may also appear when the organic polyanion is replaced by negatively charged inorganic platelets such as clay or titanate platelets.^{9–16} This was interpreted as indication that ordered multilayers could be obtained by the LBL process.⁹ Subsequently, other studies^{10,14} suggested that the degree of internal order of such multilayers may not be so large as initially thought. In the present paper,

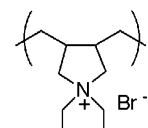


Figure 1. Chemical structure of the polycation used in this study.

we apply a set of complementary techniques, mainly atomic force microscopy and low angle X-ray scattering, to elucidate the origin of the Bragg peaks in the X-ray reflectograms of hybrid clay-based ESA multilayers, and the nature of the internal stratification of the films. In a previous work,¹⁴ the structure of such clay-based multilayers was shown to depend only slightly on the nature of the polycation used to grow the films. In the present study, we therefore concentrate exclusively on films grown from poly(diallylpyrrolidinium) bromide (Figure 1) and a synthetic hectorite (Laponite). We demonstrate that true layering is limited only to the first few nanometers of the films close to the substrate. We propose that cumulative disorder of the position of the platelets in the vertical direction is responsible for the loss of layering as the distance from the substrate increases.

Experimental Section

Materials. Poly(diallylpyrrolidinium) bromide was synthesized as described elsewhere.¹⁷ Laponite clay (60% SiO₂, 29% MgO, 0.9% Li₂O, 2.9% Na₂O; 9.8% weight loss on ignition) from Laporte Industry was a gift from Chimilab Essor (La Madeleine, France). Silicate platelets were obtained by exfoliating the clay in water, as described elsewhere.¹⁴ Silicate platelets are negatively charged, and the anionic sites are balanced by sodium cations. Platelets are approximately disk-shaped with an average diameter of 300 ± 100 Å (measured by transmission electron microscopy) and with a thickness of 9.2 Å.^{18,19}

Substrates. The substrates were one-side polished <100> silicon wafers from ACM (France) or fused silica slides (Suprasil) cut into rectangles 3 cm by 1 cm. These substrates

* To whom correspondence should be addressed.

[†] Unité de Physique et de Chimie des Hauts Polymères, Université Catholique de Louvain.

[‡] Present address: Max Planck Institute of Colloids and Interfaces, Am Mühlenberg 1, D-14476 Golm, Germany.

[§] Département de Chimie, Université Catholique de Louvain.

^{||} Present address: Fraunhofer Institut für Angewandte Polymerforschung FhG-IAP, Geiselbergstr. 69, D-14476 Golm, Germany.

were cleaned by treatment in a hot piranha solution [H_2O_2 (27%): H_2SO_4 (98%) 1:1 v/v] for 20 min (*caution: piranha solution is extremely corrosive*) and then thoroughly washed with purified water (Millipore, resistivity = 18.2 M Ω).

Preparation of Multilayers. Multilayers were self-assembled by alternately dipping the substrate for 10 min in aqueous solutions of poly(diallylpyrrolidinium) bromide (concentration of monomer units: 10^{-2} monomol L^{-1}) and of the exfoliated Laponite clay (concentration: 0.25 w %). All solutions were filtered through a 0.45 μm Millipore filter unit before use. After each dip, the substrate was rinsed by immersion into three beakers of pure water, then dried by a stream of hot air. A robotized dipping machine was used for the layer-by-layer deposition to increase reproducibility. All adsorption cycles were ended by deposition of Laponite. Multilayers obtained by dipping n times the substrate in each solution (n dipping cycles) are denoted as $\text{Si}/\{\text{P/Laponite}\}_n$ and $\text{Q}/\{\text{P/Laponite}\}_n$, depending on whether they were deposited on silicon wafers or fused silica plates, respectively.

Analytical Techniques. 1. Ellipsometry. Ellipsometric measurements were performed with a Digisel rotating compensator ellipsometer from Jobin-Yvon/Sofie Instruments (France), at a fixed incidence angle of 70° and fixed wavelength of 6328 Å. Details of the procedure are described elsewhere.⁷ An average index of refraction of 1.47 was used to analyze the data. The presence of a native oxide layer atop the silicon substrate results in an overestimation of the film thickness by about 15 Å as detailed elsewhere.⁷

2. X-ray Grazing Incidence Scattering Measurements. The experimental setup is based on a Siemens D5000 2-circles goniometer (30 cm radius). X-rays of 1.5418 Å wavelength (Cu K α) were obtained from a rotating anode. Monochromatization was achieved with the help of a secondary graphite monochromator, complemented with pulse height discrimination (scintillation counter). The scattering was measured over linear trajectories drawn in reciprocal space, either with the scattering vector perpendicular to the multilayer to obtain specular reflectivity (specular scans) or with the scattering vector tilted by α degrees away from the normal to the multilayer to measure diffuse scattering (longitudinal diffuse scans). Specular reflectivities are reported as a function of k_{z0} , the vertical component of the wavevector of the photons in a vacuum. Diffuse scattering is reported as a function of the norm of the scattering vector \mathbf{q} , which is the difference between the wavevectors in a vacuum of the outgoing and incoming photons.

Different resolutions were used by changing divergence and receiving slit widths, to integrate the scattering over different volumes of reciprocal space, $\Delta q_x \Delta q_y \Delta q_z$ (z is perpendicular to the sample, x is in the equatorial direction, and y is in the axial direction). In all cases, Δq_y was large because of large values of slit widths in the axial direction, resulting in a complete integration of the scattering cross-section in this direction. Most specular reflectivity measurements were performed with $\Delta q_{z1} = 0.0044 \text{ Å}^{-1}$ and $\Delta q_{x1} = \lambda/(4\pi) \cdot \Delta q_{z1} \cdot q$ (where q is the length of the scattering vector and λ the wavelength of the X-rays); some experiments were performed with a relaxed resolution mainly set by the equatorial size of the sample and the acceptance of the secondary monochromator, with $\Delta q_{z2} = (0.0056 + 0.138 \cdot \sin \theta) \text{ Å}^{-1}$ and $\Delta q_{x2} = \lambda/(4\pi) \cdot \Delta q_{z2} \cdot q$, where θ is the incidence angle. For simulations, an even lower resolution was also used, characterized by $\Delta q_{z3} = 0.0427 \text{ Å}^{-1}$ and $\Delta q_{x3} = \lambda/(4\pi) \cdot \Delta q_{z3} \cdot q$ (corresponding to the previous case, but ignoring the finite angular acceptance of the monochromator and the finite size of the samples).

Data were analyzed in different ways. First, a Patterson function was computed by Fourier transforming the data divided by the reflectivity of the bare substrate:²⁰

$$P(r) = \frac{1}{2\pi} \int_{-\infty}^{\infty} \frac{R(k_{z1})}{R_F(k_{z1})} e^{2ik_{z1}r} dk_{z1}$$

where k_{z1} is the component perpendicular to the interface of the wavevector in the film and $R_F(k_{z1})$ is the Fresnel reflectivity of the bare and perfectly smooth substrate computed at k_{z1} . Within the first Born approximation, this function approximates the auto-correlation of the electron density gradient along the normal to the sample,²¹ allowing for a quick overview of film structure:

$$P(r) = \frac{1}{\rho_s} \int_{-\infty}^{\infty} \frac{d\rho(z)}{dz} \frac{dr(z+r)}{dz} dz$$

where ρ_s is the electron density of the substrate and $\rho(z)$ is the electron density in the film at z . Second, a discrete model of the electron density profile of the film was fitted to the data, by adjusting the heights of slabs of 4.5 Å thickness (corresponding to the experimental resolution), the number of slabs being selected from the film thickness estimated by ellipsometry. The reflectivity was computed from this discrete electron density profile using Abeles' formalism.²² To avoid spurious oscillations appearing in the electron density profile, a regularization procedure was adopted,²³ whereby a Lagrange parameter was determined allowing to maximize the smoothness of the profile while at the same time maximizing the agreement between model and data. In addition, to increase consistency, results obtained for multilayers of smaller thickness were taken as starting points for the fits of multilayers of larger thickness.

3. Atomic Force Microscopy (AFM). AFM experiments were performed on $\text{Si}/\{\text{P/Laponite}\}_n$ films, in contact mode, with an Autoprobe CP (Park Scientific Instruments). A small size (5 $\mu\text{m} \times 5 \mu\text{m}$) scanner was employed. Images were acquired in constant force at a scan rate of 2 Hz with silicon nitride cantilevers (type A microlevers, Park Scientific Instruments, Sunnyvale, CA). Topographical images were used to determine height profiles.

Results

Figure 2a presents X-ray reflectograms obtained for a set of $\text{Si}/\{\text{P/Laponite}\}_n$ multilayers of increasing values n . The presence of only one Kiessig fringe, originating from the interference of X-rays reflected at the film/substrate and film/air interfaces, indicates the large roughness of the film/air interface. In addition, a broad Bragg reflection at 0.22 Å^{-1} , corresponding to a repeat distance of 14.4 Å, reveals the presence of internal order in the film.

This feature is made more visible by plotting the reflectivity divided by the Fresnel reflectivity of the bare substrate, Figure 2b. As demonstrated elsewhere,¹⁴ the Bragg reflection originates from the regular intercalation of the polycation between individual platelets of Laponite. The internal repeat period of the films (14.4 Å) is significantly smaller than the increment of thickness of the multilayers per dipping cycle (21 Å/cycle), computed from the linear variation of ellipsometric values of film thickness versus dipping cycle (Figure 2c). This shows that more than one layer of platelets is deposited per dipping cycle, similarly to what was reported before for other polycation/clay systems,¹⁴ or even for internally ordered multilayers made from lyotropic polyelectrolytes.⁷

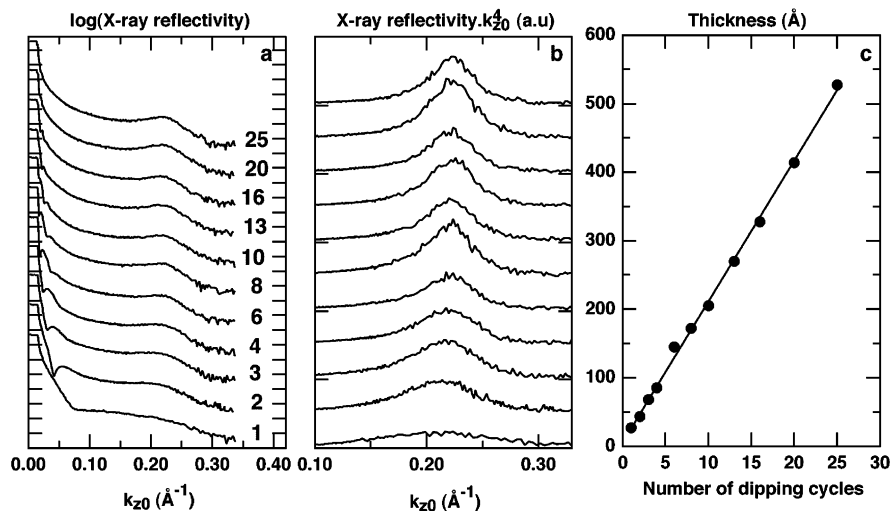


Figure 2. (a) X-ray reflectivity of Si/{P/Laponite}_n multilayers with, from bottom to top, $n = 1, 2, 3, 4, 6, 8, 10, 13, 16, 20$, and 25 . Curves are displaced vertically for clarity. (b) Zoom on the X-ray reflectivity of Si/{P/Laponite}_n multilayers, after multiplication by k_{z0}^4 . Curves are displaced vertically for clarity and are drawn in the same order as in part a. (c) Thickness of Si/{P/Laponite}_n multilayers vs number of dipping cycles, determined by ellipsometry. Included in the film thickness is a ~ 15 Å thick layer of native silicon oxide on the silicon wafer. The line is a linear fit to the data.

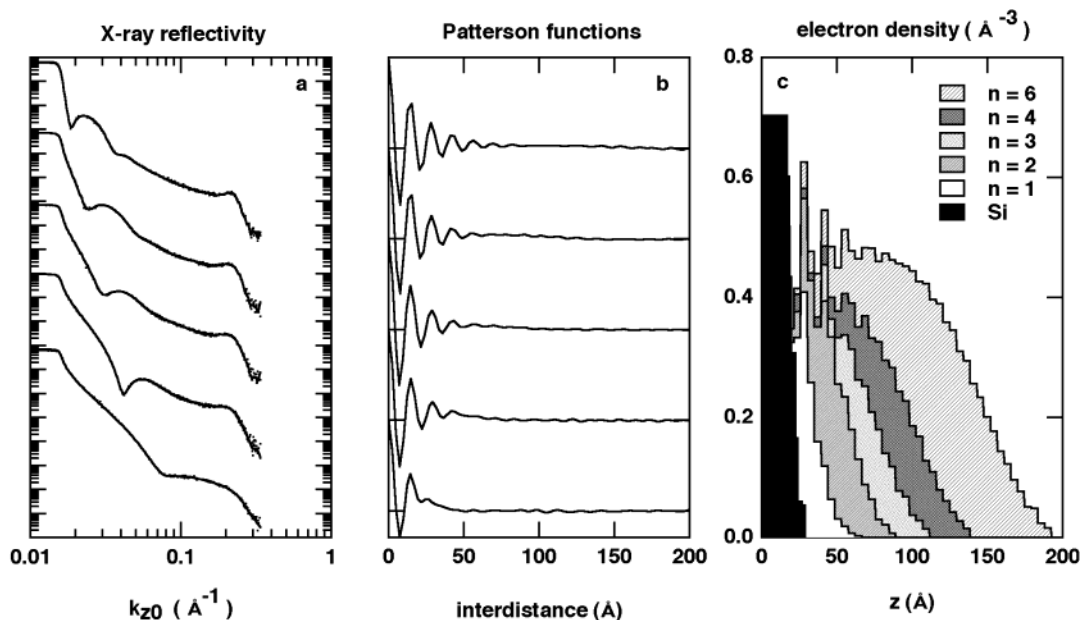


Figure 3. (a) X-ray reflectivity of Si/{P/Laponite}_n multilayers with, from bottom to top, $n = 1, 2, 3, 4$, and 6 . Curves are displaced vertically for clarity. Dots are experimental data; continuous lines are fits based on density profiles shown in part c. (b) Patterson functions computed from the reflectivity data in part a. Curves are displaced vertically for clarity and are drawn in the same order as in part a. (c) Electron density profiles obtained from the model-free fits to the experimental reflectivity shown in part a. Symbols are given in the figure.

More information on the internal structure of the films can be obtained by a detailed analysis of the X-ray reflectometry (XRR) data. Figure 3 presents X-ray reflectograms of Si/{P/Laponite}_n for increasing values of n (Figure 3a), associated Patterson functions (Figure 3b), and electron density profiles computed from these reflectograms (Figure 3c). Oscillations in the Patterson functions confirm the presence of internal order in the films. However, the oscillations are exponentially damped as the distance increases, indicating that the correlation between the vertical locations of platelets is lost after about 7 nm (similar correlation lengths were also derived from the integral widths of the Bragg peaks displayed in Figure 3a). Because of dominance of the electron density contrast between platelets and polycation and the large roughness of the film/air interface, the peak associated to the correlation between film/substrate

and film/air interfaces does not appear clearly in Patterson functions.

The analysis of electron density profiles provides even more precise information: Regularly spaced oscillations corresponding to the alternation of layers of polycations (of lower electron density) and clay platelets (of larger electron density) can be seen only close to the substrate. For larger distances, the periodic oscillations disappear, indicating the loss of layering farther away from the substrate. The progressive disappearance of density oscillations is also accompanied by an increase of oscillation width, suggesting progressive mixing between clay and polycation layers. In addition, a comparison of the profiles computed for multilayers differing by one adsorption cycle reveals that incomplete layers of clay platelets are deposited during cycle n , which are subsequently filled during cycle (n

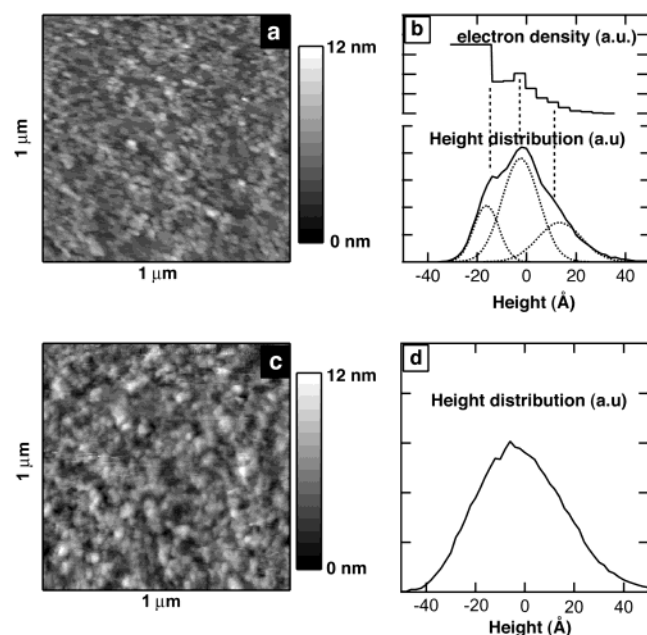


Figure 4. (a) AFM topographical image (scan = $1\ \mu\text{m} \times 1\ \mu\text{m}$) of a Si/{P/Laponite}₁ film. (b) (bottom) Height distribution of the surface obtained from image a. Dashed curves are the result of a decomposition of the height histogram into a trimodal Gaussian distribution. (top) Electron density profile determined from XRR on the same film. (c) AFM image (scan = $1\ \mu\text{m} \times 1\ \mu\text{m}$) of a Si/{P/Laponite}₂ film. (d) Height distribution of the surface obtained from image c.

+ 1) as shown by their density increase (Figure 3c). This suggests that multilayers grow by random tiling of platelets, which should create jagged profiles for the outer surface of films.

The XRR experiments on the multilayers are corroborated by AFM studies (Figure 4). Topographical images obtained for Si/{P/Laponite}₁ and Si/{P/Laponite}₂ samples (Figure 4 parts a and c, respectively) show that the surface is homogeneously covered by platelets of Laponite, as reported previously.²⁴ However, in contrast with films built from natural clays,^{24,10} no large defects are seen on the surface of the multilayers. Individual clay platelets can be observed (their size is close to the diameter measured by transmission electron microscopy, $300 \pm 100\ \text{\AA}$). The analysis of the height distribution of the surface of the Si/{P/Laponite}₁ sample reveals a trimodal distribution of heights (Figure 4b). A comparison with the electron density profile obtained from XRR (Figure 4b) indicates that the first distribution corresponds to the average height of the silicon substrate (most probably including a polycation layer), whereas the two subsequent distributions coincide with two incomplete layers of platelets spaced by about $14\ \text{\AA}$ and oriented parallel to the substrate. These results confirm that, although incomplete layers are deposited during each deposition cycle, more than one such layer is formed per dipping cycle. Moreover, height distributions broaden with increasing distance from the substrate (Figure 4b), which results in a monomodal broad distribution of heights being seen for $n \geq 2$ (Figure 4d). This observation confirms our previous conclusion from XRR that the layering tends to be lost as the distance from the substrate increases. Finally, the root-mean-square (rms) roughness of Si/{P/Laponite}_n films (determined over $4 \times 4\ \mu\text{m}^2$ images) was seen to increase strongly with n , starting at about $14\ \text{\AA}$ for $n = 1$ and saturating at about $65\ \text{\AA}$ for n greater than ~ 15 . These observations strongly suggest that random tiling of platelets is the dominant mode of growth of the multilayers.

The excellent agreement between direct space AFM measurements, which are specific to the sample outer surface, and

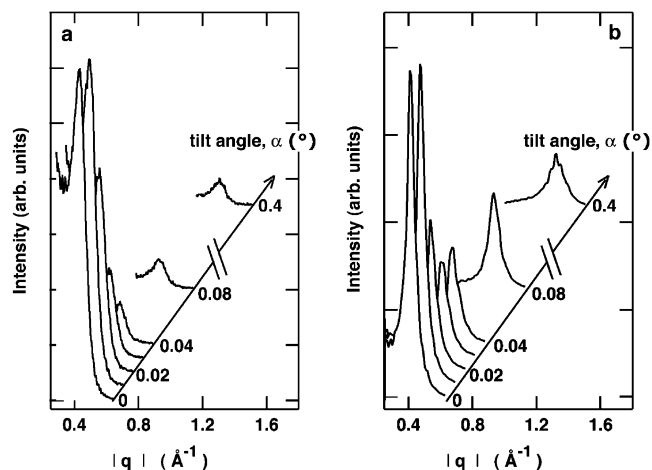


Figure 5. (a) Longitudinal diffuse scans performed on a Si/{P/Laponite}₁₆ film of about $300\ \text{\AA}$ thickness, in the region of the Bragg peak. The data are reported as a function of the norm of the scattering vector, for different tilt angles α of the scattering vector with respect to the perpendicular line to the sample. (b) Simulated longitudinal diffuse scans from the model presented in Figure 6c (multilayer of $300\ \text{\AA}$ thickness, with a Gaussian distribution of vertical distances between nearest platelets of $3\ \text{\AA}$ standard deviation and $14\ \text{\AA}$ maximum location).

reciprocal space X-ray reflectivity deductions, which provide information over the whole film thickness, limits the possibility of misinterpretation of the data. Nevertheless, none of these techniques provides direct information regarding the way platelets pack laterally within the film (or, put in another way, regarding the roughness of internal layers of platelets): XRR effectively laterally averages electron fluctuations over the coherence area of the photons (on the order of a few microns for usual collimation conditions), whereas AFM does not probe the inner part of the sample. For this reason, we addressed the issue of the inner morphology of Si/{P/Laponite}_n films by measuring the diffuse (off-specular) X-ray scattering of the multilayers. Contrasting with specular reflectivity which is sensitive only to the vertical fluctuations of the laterally averaged electron density, the diffuse scattering provides information on electron density fluctuations in the horizontal direction.^{25,26}

Longitudinal diffuse scans performed on a Si/{P/Laponite}₁₆ film are reported in Figure 5a, in the region of the Bragg peak. The Bragg peak is seen first to decrease rapidly as the scattering vector is inclined from the perpendicular to the sample and then to decrease much more slowly for tilt angles above 0.04° , being still about 5% of the specular Bragg reflection for a tilt angle of 1° (data not shown). This off-specular component may be due to random tilting of the platelets, to randomness of the vertical position of platelets with respect to horizontal neighbors, or to both.

To clarify the origin of diffuse scattering, we simulated the scattering by generating randomly sets of 50 multilayers, computing their scattering in the first Born approximation, and averaging the results. The random placement of the platelets in the multilayer was only considered, neglecting in a first step the possible tilting of platelets. The distribution of the platelets in the film was assumed to obey the following rules: (1) the vertical distance between two neighboring platelets (or between a platelet and the neighboring substrate) is distributed randomly according to a Gaussian distribution centered about $14\ \text{\AA}$ and of standard deviation σ ; (2) and the distance between the edges of two neighboring platelets in the horizontal plane is distributed randomly according to a box distribution of $300\ \text{\AA}$ width.

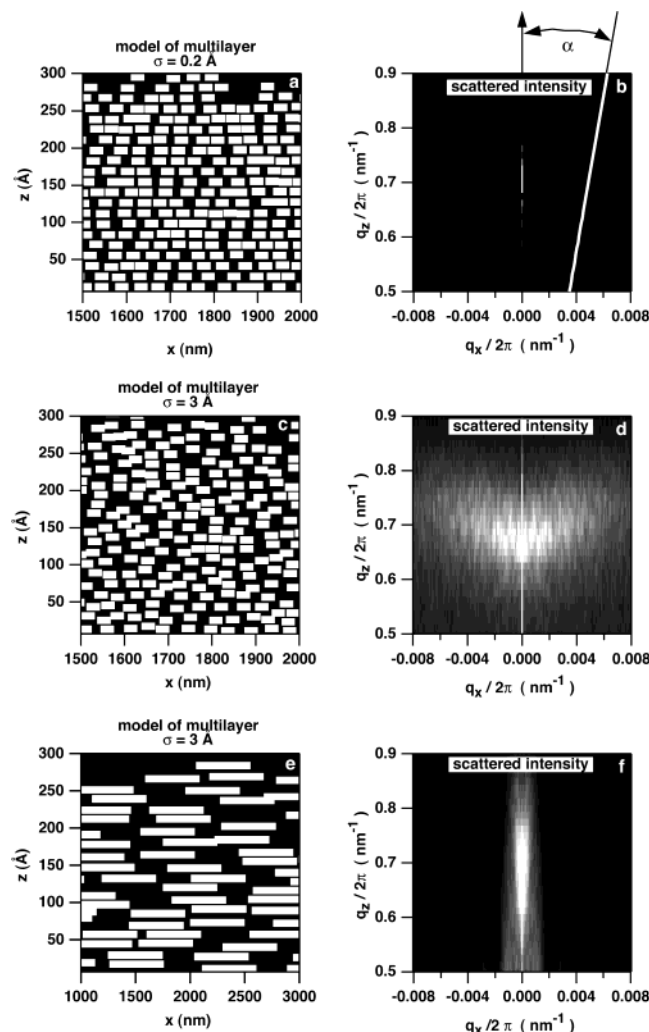


Figure 6. (a, c, and e) Enlarged views of the cross-section of multilayers from the simulations. Platelets (white) are positioned according to Gaussian distributions of vertical distances between nearest neighbors with 14 Å average repeat distance and standard deviations of, respectively, 0.2, 3 and 3 Å. The lateral size of the platelets is 30 (a and c) or 500 nm (e). Note the difference of scale in z and x directions and the smaller scale used for the x direction of part e. (b, d, and f) Average scattering cross-sections in the region of the Bragg peak, obtained from the simulation of 50 multilayers of characteristics identical to the ones depicted in parts a, c, and e, respectively. The scattering cross-sections are represented in false gray colors, as a function of the x and z components of the scattering vector \mathbf{q} . The white line in part b indicates the trajectory followed in reciprocal space during a typical longitudinal diffuse scan.

Platelets were taken to be 9 Å thick and 300 Å wide. The whole process was repeated for different thickness of the simulated multilayers.

Figure 6a presents a zoom on a typical cross-section of a so-generated multilayer (300 Å thick), whereas Figure 6b is an image of the average scattering of a set of 50 similar multilayers, in the region of the Bragg peak. The low value of σ selected for this case (0.2 Å) results in almost perfect layering of the platelets over the whole film thickness. As a consequence, the scattering is essentially concentrated along the specular line ($q_x = 0$). Parts c and d of Figure 6 present similar images for the case where significant disorder occurs in the packing of the platelets in the vertical direction ($\sigma = 3$ Å, close to the case of Laponite-based multilayers, see below). The Gaussian distribution of platelets in the vertical direction results in true layering of the platelets only close to the substrate. As a result of the

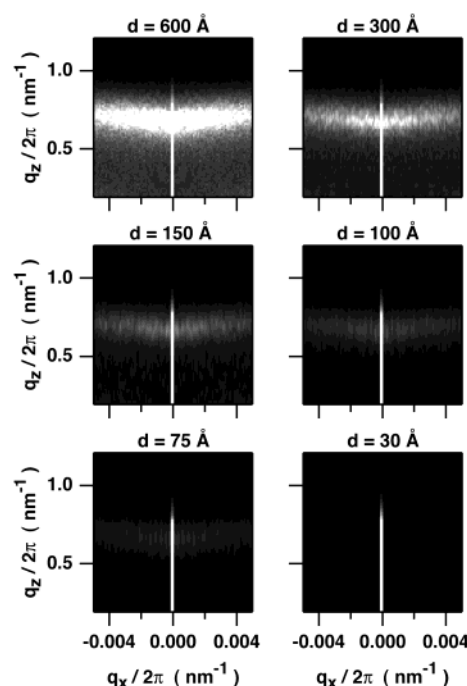


Figure 7. Average scattering cross-sections in the region of the Bragg peak, obtained from simulations of sets of multilayers of increasing thickness, d , deposited on a perfectly flat substrate.

“internal roughness” of the multilayer, significant off-specular scattering now appears (away from the specular scattering line, $q_x = 0$).

Longitudinal diffuse scans were also obtained from the simulations. Figure 5b presents results from simulations performed for a multilayer of a thickness close to the sample Si/{P/Laponite}₁₆, again with $\sigma = 3$ Å for the distribution of vertical distances between platelets. This corresponds to the scattering cross-section presented in Figure 6d. These simulated results may be compared with the experimental data of the sample Si/{P/Laponite}₁₆ in Figure 5a. Given the simplicity of the model, the agreement between both sets of data, experimental and simulated, is satisfactory.

Figure 7 presents the simulated scattering cross-sections of multilayers of increasing thickness, taking $\sigma = 3$ Å for the vertical distribution of platelet distances. When the thickness of the multilayer increases, the relative importance of diffuse scattering also increases as compared to the specular component. This results from the fact that true layering of the platelets only occurs close to the substrate: Rough “layers” farther away from the substrate essentially contribute to the diffuse scattering, whereas true layers of platelets close to the substrate contribute dominantly to the specular component (even though these contribute also slightly to the off-specular component due to the finite lateral extension of the platelets). In a specular scan, the diffractometer effectively integrates the scattering cross-section over some finite resolution volume, depending on slit sizes, characteristics of the monochromator, etc. For the high resolution used in typical reflectometry setups, the diffractometer will integrate over a volume of restricted extent in the q_x direction, essentially excluding the diffuse component from the measurement for Si/{P/Laponite}_n multilayers. Therefore, outer “layers” will contribute less to the measurement than true layers close to the substrate. By contrast, if the resolution is decreased, increasing amounts of diffuse scattering will be included in the measurements. This will decrease the relative importance of layers close to the substrate, as compared to “layers” further apart. Therefore, it is possible to evaluate the layering of the

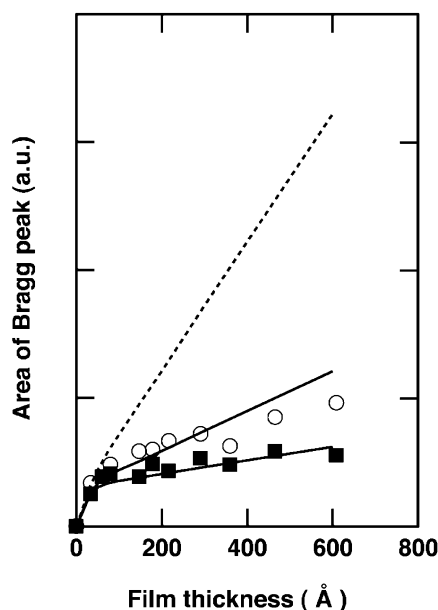


Figure 8. Variation of the area of the Bragg peak with thickness for $\text{Si}/\{\text{P/Laponite}\}_n$ films. Circles correspond to specular measurements of different resolution (open circles, high resolution of reflectivity measurements; closed circles, resolution relaxed by a factor of about 3). The dashed line indicates what would have been obtained with our diffractometer, had we relaxed further the resolution.

platelets in the samples by plotting the areas of the Bragg peaks (measured in a specular scan) as a function of multilayer thickness (or, equivalently, number of dipping cycles) for different resolutions of the experimental setup.

The variation of the area of the Bragg peak (normalized to unit scattering surface) with thickness of the $\text{Si}/\{\text{P/Laponite}\}_n$ films is presented in Figure 8 for two resolutions of the diffractometer (a high resolution defined by a resolution volume $\Delta q_{x1} \cdot \Delta q_{z1}$ defined in the Experimental Section and a lower resolution defined by a larger resolution volume $\Delta q_{x2} \cdot \Delta q_{z2}$). Both curves first show a rapid increase with film thickness, followed by a slower variation rate above a thickness of about 75 Å. The continuous lines in the figure were obtained by performing the integration over the corresponding resolution volumes of the simulated scattering cross-sections of the set of multilayers of Figure 7.

Again, the agreement between experimental data and simulations is reasonably good. The decrease of the slope of the curves in Figure 8 corresponds to the loss of true layering as the distance from the substrate increases or, equivalently, to the fact that the rough "layers" of platelets farther away from the substrate essentially contribute to the diffuse scattering. The dashed curve in Figure 8 indicates what would have been obtained for an even lower resolution $\Delta q_{x3} \cdot \Delta q_{z3}$ (which could not be attained experimentally with our setup, due to limitations set by the secondary monochromator). In this case, the Bragg peak would have evolved almost linearly with film thickness, because the detector would now have accepted most of the diffuse scattering in addition to the specular component.

To confirm that the true specular scattering originates mainly from the very first layers of platelets close to the substrate, we compared two samples (16 dipping cycles) grown on two substrates of different initial roughness: a silicon substrate of ~ 2 Å rms roughness and a fused silica substrate of 15 Å rms roughness, as determined by X-ray reflectometry. The inspection of the reflectograms (Figure 9) clearly shows that the intensity of the Bragg peak strongly decreases for the multilayer self-

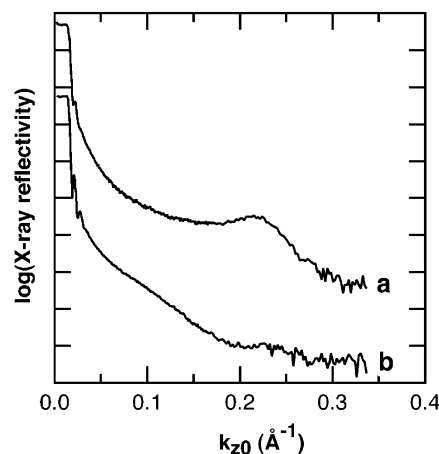


Figure 9. X-ray reflectivity of $\text{Si}/\{\text{P/Laponite}\}_{16}$ (a) and $\text{quartz}/\{\text{P/Laponite}\}_{16}$ (b) multilayers, showing the effect of substrate roughness on the Bragg reflection. Curves are displaced vertically for clarity.

assembled on the "rough" fused silica substrate, for which no layering of the platelets even close to the substrate can be expected.

Discussion

The main observations obtained by the present study on $\text{Si}/\{\text{P/Laponite}\}_n$ multilayers are the following: 1. Incomplete layers of platelets are formed during one cycle of deposition, as revealed by the electron density profiles from XRR and by the AFM observations. 2. Despite this, more than one (incomplete) layer of platelets are simultaneously deposited per dipping cycle, as shown by the large thickness increment per dipping cycle (21 Å) compared to the repeat distance between platelets (14.4 Å), and by AFM results on the $\text{Si}/\{\text{P/Laponite}\}_1$ film. 3. The roughness of the multilayers is large, as shown by XRR or AFM. For instance, the rms roughness of a multilayer of 300 Å thickness amounts to 65 Å, which is more than 20% of the total thickness. 4. True layering of the platelets only occurs close to the substrate, and no layering appears farther than about 75 Å from the substrate. If a rougher substrate is used, layering does not even occur. 5. The experimental scattering data, diffuse and specular, can be represented by a model wherein the distance between neighboring platelets is described by a random Gaussian distribution of 3 Å standard deviation. The accumulation of such random deviations results in a loss of true layering as the distance from the substrate increases.

These observations fit well to a simple model of growth, consisting in the random tiling of platelets over a soft polycationic cushion. To explain the deposition of multiple incomplete "layers" of platelets, separated by a polyelectrolyte layer (as demonstrated in a previous study¹³), the polycation must exhibit by necessity some ability to reorganize during platelet deposition, i.e., the polycation "layer" must display some mobility. This means that the multilayer build-up does not proceed by the simple alternate deposition of individual layers of polycation or platelets but implies a limited reorganization of different "layers" during the adsorption step, as was proposed by Kleinfeld et al.⁹ This behavior, which was reported for other systems,^{7,27} contrasts with the idealized layer-by-layer growth described for {organic/inorganic} multilayers incorporating α -ZrP platelets.²⁸ In the case of clays, the complex growth process leads to a film which should be more correctly considered as a nanocomposite with preferential orientation of the platelets than as a true multilayer. This is not surprising, as

no one would imagine to create a well ordered pavement simply by throwing granite plates at random on a mobile and soft cushion.

The limited extent of layering is not incompatible with the notion of stratified multilayers, if, by the term "stratification", reference is made to the fact that a given platelet will be located at a position defined by the sequence of dipping cycles and will not move with time. However, given the large roughness of Laponite/polycation multilayers, the uncertainty on the exact location of a platelet will also be large, on the order of ± 65 Å for sufficiently thick films. This will be even worse for films grown from natural clays, whose larger roughness was demonstrated by previous studies.²⁴

Finally, this study indicates how cautious one should be when attempting to evaluate the quality of multilayers by looking to the characteristics of the Bragg reflection in specular scans. As demonstrated in Figure 8, the way the area of the Bragg peak varies with film thickness is strongly sensitive to the experimental resolution of the diffractometer: for low resolution, inclusion of the diffuse scattering in the measured intensity will result in a linear variation of the area of the Bragg peak with film thickness, notwithstanding the internal disorder of the film. This effect will be much more pronounced when using platelets of larger lateral extent, such as found for natural clays. Figure 6f presents the simulated scattering of a set of multilayers whose internal structure is displayed in Figure 6e. The simulation was performed with platelets of 500 nm lateral extent, as opposed to the 30 nm used for the previous simulations (Figure 6c,d). The lateral expansion of the structure of the multilayer logically results in the contraction of reciprocal space in the horizontal direction by a reciprocal factor. As a consequence, even with a high resolution diffractometer, a large fraction of the diffuse scattering will be included in specular measurements of such multilayers. The area of the Bragg peak will thus vary close to linearly with film thickness. Therefore, such an observation does not imply automatically that true layering occurs anywhere in the film, but possibly only close to the substrate. This may explain why other studies of hybrid systems made with platelets of larger lateral size than Laponite reported a continuous increase of the intensity of Bragg peak with the number of dipping cycles.¹²

Finally, we briefly turn to the effect of possible tilts of the platelets in the film. As tilting would also result in the disruption of layering and would provide a diffuse scattering similar to the one generated by rough "layers", it is not easy to distinguish between tilting of platelets and randomization of the placement of the platelets in the vertical direction. However, examination of AFM images, including a comparison of height-height correlation functions,²⁶ did not allow us to conclude positively about significant tilting of the platelets. We thus conclude that, although limited tilting most probably occurs in the films, it does not provide significant differences compared to random placement of the platelets in the film.

Conclusions

By combining ellipsometry, AFM, and specular and off-specular grazing angle X-ray scattering measurements, we obtained a complete set of data, in both direct and reciprocal spaces, on the structure of $\{P/Laponite\}_n$ multilayers. The whole set of data can be consistently described by a simple model of multilayer growth, consisting in the random tiling of negatively charged clay platelets onto a dynamic cushion of the organic polyelectrolyte. As a result of this random and dynamic process,

platelets pack according to a distribution of vertical distances between nearest neighbors, centered about 14 Å and of ~ 3 Å standard deviation. The accumulation of such random fluctuations in the vertical direction leads to the loss of layering of the platelets farther than about 75 Å from the substrate. In this respect, most of the film should be considered as a nanocomposite with preferential orientation of the platelets, rather than as a true multilayer. This model is quantitatively supported by simulations of the specular and off-specular scattering of such multilayers.

Acknowledgment. The authors thank P. Fischer (UCL) for the synthesis of poly(diallylpyrrolidinium) as well as B. Nysten (UCL) for his assistance with AFM measurements. The research was financially supported by the DG Recherche Scientifique of the French Community of Belgium (Action de Recherches Concertées 00/05-261).

Supporting Information Available: A description of the simulation method used to generate Figures 5–8 is available free of charge via the Internet at <http://pubs.acs.org>.

References and Notes

- (1) Arys, X.; Jonas, A. M.; Laschewsky, A.; Legras, R. In *Supramolecular Polymers*; Ciferri, A., Ed.; Marcel Dekker: New York, 2000; p 505.
- (2) Bertrand, P.; Jonas, A. M.; Laschewsky, A.; Legras, R. *Macromol. Rapid Comm.* **2000**, *21*, 319.
- (3) Decher, G. *Science* **1997**, *277*, 1232.
- (4) Schlenoff, J. B.; Ly, H.; Li, M. *J. Am. Chem. Soc.* **1998**, *120*, 7626.
- (5) Yoo, D.; Shiratori, S. S.; Rubner, M. F. *Macromolecules* **1998**, *31*, 4309.
- (6) Philipp, B.; Dautzenberg, H.; Linow, K.-J.; Kötz, J.; Dawydoff, W. *Prog. Polym. Sci.* **1989**, *14*, 91.
- (7) Arys, X.; Laschewsky, A.; Jonas, A. M. *Macromolecules* **2001**, *34*, 3318.
- (8) Joly, S.; Kane, R.; Radzilowski, L.; Wang, T.; Wu, A.; Cohen, R. E.; Thomas, E. L.; Rubner, M. F. *Langmuir* **2000**, *16*, 1354.
- (9) Kleinfeld, E. R.; Ferguson, G. S., *Science* **1994**, *265*, 370.
- (10) Kotov, N. A.; Haraszti, T.; Turi, L.; Zavala, G.; Geer, R. E.; Dékány, I.; Fendler, J. H. *J. Am. Chem. Soc.* **1997**, *119*, 6821.
- (11) Kaschak, D. M.; Mallouk, T. E. *J. Am. Chem. Soc.* **1996**, *118*, 4222.
- (12) Sasaki, T.; Ebina, Y.; Watanabe, M.; Decher, G. *Chem. Commun.* **2000**, *21*, 2163.
- (13) Sasaki, T.; Ebina, Y.; Tanaka, T.; Watanabe, M.; Decher, G. *Chem. Mater.* **2001**, *13*, 4661.
- (14) Glinel, K.; Laschewsky, A.; Jonas, A. M. *Macromolecules* **2001**, *34*, 5267.
- (15) Glinel, K.; Laschewsky, A.; Jonas, A. M. *Langmuir* **2002**, *18*, 1408.
- (16) Vuillaume, P. Y.; Jonas, A. M.; Laschewsky, A. *Macromolecules* **2002**, *35*, 5004.
- (17) De Vynck, V.; Goethals, E. J. *Macromol. Rapid Commun.* **1997**, *18*, 149.
- (18) Ramsay, J. D. F. *J. Colloid Interface Sci.* **1986**, *109*, 441.
- (19) Ramsay, J. D. F.; Linder, P. J. *Chem. Soc., Faraday Trans.* **1993**, *89*, 4207.
- (20) Bollinne, C.; Stone, V. W.; Carlier, V.; Jonas, A. M. *Macromolecules* **1999**, *32*, 4719.
- (21) Pershan, P. S.; Als-Nielsen, J. *Phys. Rev. Lett.* **1984**, *52*, 759.
- (22) Lekner, J. *Theory of Reflection of Electromagnetic and Particle Waves*; Martinus Nijhoff Publishers: Dordrecht, The Netherlands, 1987.
- (23) Press, W. H.; Teukolsky, S. A.; Vetterling, W. T.; Flannery, B. P. *Numerical Recipes in C*, 2nd ed.; Cambridge University Press: Cambridge, U.K., 1992.
- (24) van Duffel, B.; Schoonheydt, R. A.; Grim, C. P. M.; De Schryver, F. C. *Langmuir* **1999**, *15*, 7520.
- (25) Tolan, M. *X-ray Scattering from Soft-Matter Thin Films*; Springer Tracts in Modern Physics; Springer: Berlin, 1999; Vol. 148.
- (26) Daillant, J.; Gibaud, A. *X-ray and Neutron Reflectivity: Principles and Applications*; Springer: Berlin, 1999.
- (27) Koetse, M.; Laschewsky, A.; Jonas, A. M.; Wagenknecht, W. *Langmuir* **2002**, *18*, 1655.
- (28) Kim, H. N.; Keller, S. W.; Mallouk, T. E.; Schmitt, G.; Decher, G. *Chem. Mater.* **1997**, *9*, 1414.